

Soft Tail-dropping for Adaptive Visual Tokenization

Zeyuan Chen¹ Kai Zhang² Zhuowen Tu¹ Yuanjun Xiong²
¹UC San Diego ²Adobe

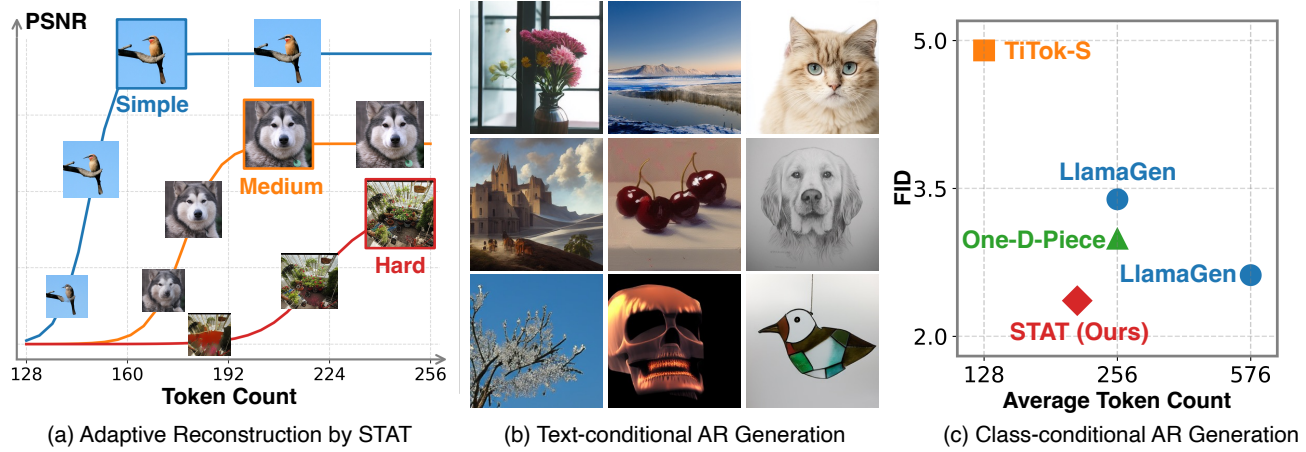


Figure 1. (a) **STAT adaptively allocates token counts based on image complexity** (the outlined figures), using fewer tokens for simple images and more for complex ones. When paired with a vanilla autoregressive model, STAT enables (b) **high-quality text-conditional image generation** and (c) **the best FID in class-conditional generation** on ImageNet among visual tokenizers.

Abstract

We present **Soft Tail-dropping Adaptive Tokenizer (STAT)**, a 1D discrete visual tokenizer that adaptively chooses the number of output tokens per image according to its structural complexity and level of detail. STAT encodes an image into a sequence of discrete codes together with per-token keep probabilities. Beyond standard autoencoder objectives, we regularize these keep probabilities to be monotonically decreasing along the sequence and explicitly align their distribution with an image-level complexity measure. As a result, STAT produces length-adaptive 1D visual tokens that are naturally compatible with causal 1D autoregressive (AR) visual generative models. On ImageNet-1k, equipping vanilla causal AR models with STAT yields competitive or superior visual generation quality compared to other probabilistic model families, while also exhibiting favorable scaling behavior that has been elusive in prior vanilla AR visual generation attempts.

1. Introduction

Autoregressive models have demonstrated remarkable success across modalities - powering large language models (LLMs) [43, 58] in text and achieving strong performance in visual generation for both images and videos [6], as well as joint modeling of language, vision, and beyond [8–10]. Being the cornerstone of this success, modern text tokenizers [44, 53] demonstrate the intriguing property that its representation cardinality is dependent on the content it is representing. This property of content-dependent compression, is unsurprisingly also the hallmark of modern image and visual compression approaches. However, tokenizers for popular visual generation models [5, 42, 56] still anchor the visual tokens on rigid 2D structure and enforce fixed compression ratio regardless of the image and video content. Consequently, simple images may be over-represented, while complex scenes may remain under-encoded, which in turn challenges the capability of the generative models. Despite numerous efforts [2, 27, 40, 48, 68] to decouple the representation cardinality of visual tokenizer from the input resolution, we have not achieved

adaptive alignment of output token cardinality with the visual complexity. We also have not observed empirically the compatibility of content-adaptive visual tokenizers with generative models, especially autoregressive generative models, which is well suited for tokenizers with this property [6, 43].

In this work, we propose STAT, which uses soft tail-dropping for adaptive visual tokenization. In detail, as a tokenizer, STAT is able to encode a given image into discrete latent tokens, decide the token counts used for a given image, and use the corresponding token counts for decoding. Concretely, STAT introduces a probabilistic token dropout module that predicts keep probabilities for each token position, followed by per-token Bernoulli sampling to decide whether a token is kept or dropped. To guide the learning process for the dropout probabilities, we apply three priors: (1) the probability profile should be monotonically decreasing, enforcing a tail-shaped dropping pattern; (2) the sum of predicted probabilities should correlate with image complexity, assigning fewer tokens to simple images and more to complex ones; and (3) the model should attempt to use fewer tokens to increase the compression ratio. These priors induce a model providing adaptive compression over images, which is demonstrated to have fewer average token count but better reconstruction.

More importantly, the adaptivity of STAT facilitates ease of modeling for generative models. When integrated with a vanilla autoregressive model that performs next token prediction, STAT enables the model to reach state-of-the-art generation quality, comparable to or surpassing diffusion-based models and other autoregressive models deviating from the simple next token prediction paradigm.

To summarize, our contributions are:

- We propose STAT, an adaptive visual tokenizer that dynamically determines the compression ratio with different token counts based on image complexity.
- We introduce to learn a probabilistic soft tail-dropping strategy that enables the tokenizer to adaptively allocate token counts to different images, leading to improved robustness in generative modeling.
- STAT achieves the state-of-the-art reconstruction performance with fewer average tokens used. Integrating STAT into a vanilla autoregressive framework yields a strong generative model comparable with other state-of-the-art generative models.

2. Related Work

2.1. Image Tokenization

Image tokenization is one important step in modern visual generative models [5, 31, 49], where the images are mapped from the pixel space into a compressed high-dimensional latent space, either continuous or discrete, to avoid pro-

hibitive computation in pixel-space and smoothen the distribution to be modeled. Variational Autoencoder (VAE) [29] is one representative continuous tokenizer that maps images into a continuous latent space. Vector-quantized autoencoder (VQ-VAE) [60] pioneers discrete visual tokenization. It consists of an encoder, a quantizer with a codebook at the bottleneck, and a decoder. The quantizer maps the encoded continuous embeddings into codebook embeddings by nearest neighbor search, and the discretized embeddings are fed to the decoder for reconstruction. Improvements to VQ-VAEs have been widely explored, including architecture [7, 31, 46, 65], training objectives [16, 45], and quantization techniques [15, 39, 66, 71].

VQ tokenizers typically maintain a 2D spatial structure, where the downsampled 2D features at the bottleneck are discretized. To decouple the token number from input dimension, 1D tokenizers like TiTok [27, 68] propose to concatenate 2D patch embeddings with 1D latent tokens as the model input and distill information from patch embeddings into 1D latent tokens, which are then quantized. Flexible tokenizers [2, 40, 64] are subsequently developed to learn ordered 1D token representation with nested dropout [48], allowing representing images with a varying number of tokens. These methods still employs a predetermined token count in their inference. STAT learns to reconstruct images with content-adaptive token counts, representing an image with the number of tokens aligned with its complexity.

Among emerging works investigating adaptive tokenizers, ALIT [14] proposes to iteratively update the 1D token sequences to identify smallest number of tokens for a given image, but it requires multiple forward passes. One concurrent work [13] uses post-hoc heuristics based on reconstruction of the full-length tokens to determine the token count after the encoding. In contrast, STAT is single-pass and aligns token cardinality prediction with image complexity via an explicit objective, rather than treating token count as a fixed hyperparameter or a heuristic byproduct. We also demonstrate that STAT is particularly suitable for vanilla autoregressive models, achieving compelling generation quality that scales favorably with the capacity of generative models.

2.2. Image Generation

Generative adversarial network (GAN) [20] is one representative framework for early image generation. Many subsequent works [3, 26, 51] have been proposed to advance GANs in both fidelity and diversity. More recently, diffusion models [4, 25, 38, 42, 49, 54, 69] have become a popular choice for image generation due to their excellent generation quality and stable training.

With the development of VQ-VAE and other discrete tokenizers, discrete generative models have also gained attention in recent years, which can be mostly divided into two

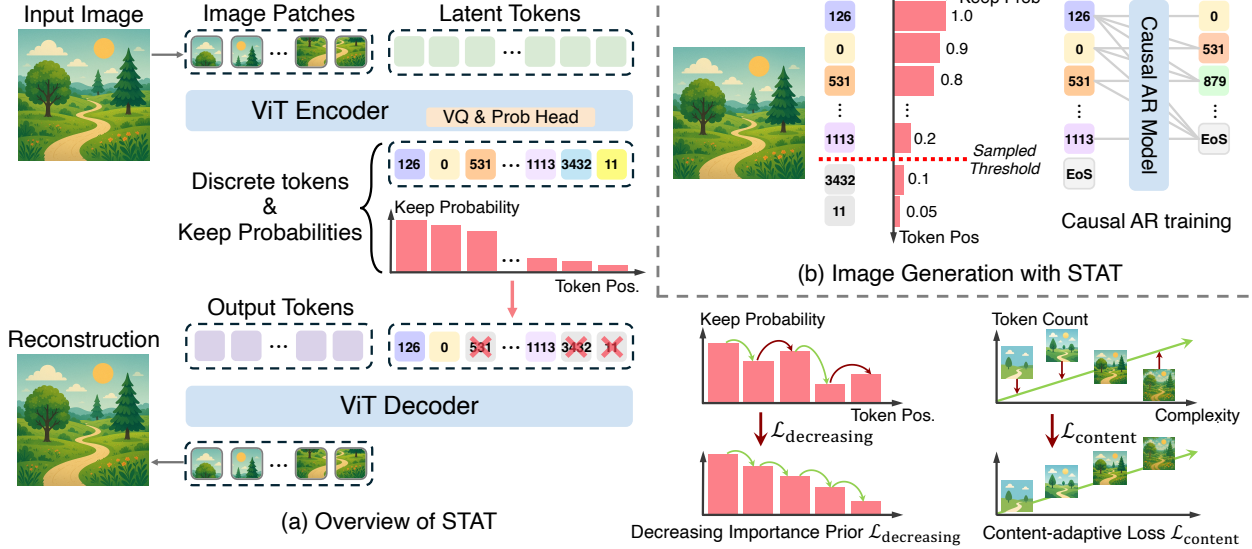


Figure 2. (a) **Overview of STAT.** A ViT encoder followed by a vector-quantizer (VQ) layer produces discrete latent tokens along with a keep probability for each token position. Probabilistic token dropping is applied to obtain a masked latent sequence for reconstruction, while two regularization losses enforce content-adaptive allocation and a decreasing importance prior. (b) **Image generation with STAT.** A special End-of-Sequence (EoS) token enables adaptive-length autoregressive generation, where the EoS position is determined by a threshold with the keep-probability profile predicted by STAT.

categories. BERT-style models [5, 32, 66] that typically use an Transformer encoder architecture with bi-directional attention and sample tokens in random order to gradually unmask all tokens in generation. Another category, GPT-style autoregressive generative models [16, 31, 56, 65] are based on decoder-only architectures with causal attention. It features easy integration with other modalities such as language. LlamaGen [56] is one representative work in this category, which demonstrates that with powerful image tokenizers and scalable model architectures, autoregressive model can reach competitive performance with diffusion models, albeit still hitting scaling bottleneck with respect to the model capacity.

Recently there have been numerous efforts in exploring new autoregressive-like pipelines for visual generation. VAR [57] models the autoregressive learning on images as next-scale prediction to form a coarse-to-fine generation process. MAR [33] introduces a diffusion loss to BERT-style generative models to allow using continuous tokenizers. RandAR [41] and xAR [47] augment next token prediction with different variations to strengthen decoder-only autoregressive visual generation. We note that these methods, while achieving strong generation performance, require additional effort [10, 21, 72] to unite with LLMs.

3. Method

Our goal is to build a visual tokenizer that allocates *content-adaptive* numbers of latent tokens. This requires mov-

ing beyond fixed 2D image grids and learning a 1D latent sequences whose lengths are determined adaptively by the input complexity. STAT addresses this through a two-stage training pipeline. First, the tokenizer learns prefix-robust reconstruction via randomized tail truncation, producing an ordered latent sequence. Second, it becomes content-adaptive by predicting per-token keep probabilities and learning a soft tail-dropping policy driven by visual complexity. This enables STAT to assign more tokens to complex images and fewer to simple ones, and naturally supports 1D auto-regressive (AR) visual generation.

3.1. Architecture

STAT adopts a 1D Transformer-based tokenizer that decouples tokens from fixed 2D grids, enabling decoding with variable-length latents and adaptive token allocation.

Given an image $x \in \mathbb{R}^{B \times C \times H \times W}$, a patch embedding layer maps it to $\mathbf{P} \in \mathbb{R}^{B \times N \times D}$, where $N = H/f \cdot W/f$ for downsampling factor f . We concatenate \mathbf{P} with L learnable latent tokens $\mathbf{L} \in \mathbb{R}^{B \times L \times D}$ and encode the full sequence:

$$[z_p, z_l] = \text{Enc}([\mathbf{P}, \mathbf{L}]). \quad (1)$$

where z_p and z_l are output patch tokens and latent tokens. We only retain z_l and the vector-quantizer maps each latent token from z_l to the nearest codebook entry, yielding discrete latents z_q . The decoder reconstructs the image from z_q and a set of learnable output tokens \mathbf{O} :

$$\hat{x} = \text{Dec}([z_q, \mathbf{O}]). \quad (2)$$

This architecture distills any input image into a 1D token sequence, making STAT compatible with both flexible prefix reconstruction (Sec. 3.2.1) and content-adaptive token allocation (Sec. 3.2.2).

3.2. Adaptive Visual Tokenizer

STAT is trained in two stages. In the first stage (Sec. 3.2.1), the tokenizer learns to reconstruct images from *flexible* prefix lengths, but the selection of token count is externally randomized and not conditioned on content. In the second stage (Sec. 3.2.2), STAT becomes *content-adaptive*, learning to allocate token counts based on image complexity through a probabilistic soft tail-dropping mechanism.

3.2.1. Flexible Prefix Reconstruction

Before learning content adaptivity, we first train the tokenizer to reconstruct images from *any* prefix of its 1D latent sequence. Following prior work [2, 40], STAT is trained with *hard tail-dropping*: in each iteration, a keep length $K \sim \mathcal{U}(L_{\min}, L_{\max})$ is sampled from a uniform distribution and the first K quantized tokens are used for reconstruction:

$$\hat{x} = \text{Dec}([z_q \odot m, \mathbf{O}]), \quad m_i = \mathbf{1}[i < K].$$

Random prefix truncation induces an *ordered* token representation in which early tokens encode coarse global structure, while later tokens refine details. This stage enables STAT to reconstruct images from prefixes of latent token sequences, but does *not* teach the tokenizer to determine how many tokens each image should use.

3.2.2. Content-Adaptive Token Allocation

To make token counts adaptive to visual complexity, STAT learns to predict a per-token keep-probability profile for each image and applies probabilistic soft tail-dropping.

Per-token Keep Probabilities. We design our encoder to output latent tokens $z_l \in \mathbb{R}^{B \times L \times D}$ along with their per-token keep probability by:

$$p_{j,i} = \sigma(g_\theta(z_l[j, i])). \quad (3)$$

where j indexes the batch dimension and i indexes the token position. g_θ is a position-aware multilayer perception (MLP), and σ denotes the sigmoid function. The resulting probabilities form a *token importance profile* over positions. Each token is stochastically retained via independent Bernoulli sampling $m_{j,i} \sim \text{Bernoulli}(p_{j,i})$, and reconstruction is performed from the masked discrete latent sequence $z_{q,j} \odot m_j$, where $m_j = [m_{j,1}, m_{j,2}, \dots, m_{j,L}]$ is the dropping mask for the image x_j . Since Bernoulli sampling is non-differentiable, we adopt a straight-through estimator (STE) to allow gradient flow during training.

We can also compute the expected number of retained

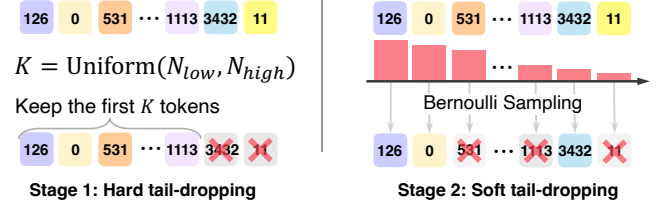


Figure 3. Token dropping strategies in two training stages.

tokens for image x_j by:

$$T_j = \sum_{i=0}^{L-1} p_{j,i}, \quad (4)$$

so token allocation becomes a differentiable function of the continuous importance landscape rather than a discrete selection problem, hence the name ‘soft tail-dropping’.

Content-adaptive prior. To allocate tokens based on visual complexity, we impose a prior that encourages the expected token count to increase with perceptual difficulty. For each image x_j , we compute its perceptual reconstruction error $L_{\text{perc},j}$ (e.g., LPIPS) as a proxy for visual complexity, and correlate this quantity with the expected token count T_j . Across all samples in a batch, we optimize

$$\mathcal{L}_{\text{content}} = (1 - \text{corr}(L_{\text{perc}}, T))^2, \quad (5)$$

which encourages a strong positive correlation between the complexity proxy L_{perc} and the allocated token count T . $\mathcal{L}_{\text{content}}$ acts as a *content-adaptive prior* on token counts, nudging the tokenizer to assign more tokens to harder images and fewer tokens to simpler ones. By contrasting all samples in the batch, this loss encourages the model to properly allocate tokens without the need to normalize the complexity proxy precisely. In practice, we compute the correlation using the Pearson correlation coefficient.

Decreasing Importance Prior. To match the causal structure prior required for autoregressive generation, we regularize the importance profile toward a decreasing form by penalizing upward steps:

$$\mathcal{L}_{\text{decrease}} = \sum_{i=1}^{L-1} \max(0, p_{j,i} - p_{j,i-1}). \quad (6)$$

This encourages a soft monotonic decay along positions, stabilizes variable-length decoding, and produces consistent, content-dependent early-stop behavior when the tokenizer is used in AR models for generation.

KL Sparsity Prior. The content adaptive loss shapes *relative* allocation but does not enforce a global token budget. We impose a Bernoulli sparsity prior by regularizing the av-

verage keep probability:

$$\bar{p}_j = \frac{1}{L} \sum_{i=0}^{L-1} p_{j,i} \quad (7)$$

toward a target preset sparsity p^* using KL divergence:

$$\mathcal{L}_{\text{sparse}} = \text{KL}(\text{Bern}(p^*) \parallel \text{Bern}(\bar{p}_j)). \quad (8)$$

Overall Objective The adaptive tokenizer is trained with the composite loss

$$\begin{aligned} \mathcal{L} = & \mathcal{L}_{\text{recon}} + \mathcal{L}_{\text{GAN}} + \mathcal{L}_{\text{VQ}} + \lambda_{\text{content}} \mathcal{L}_{\text{content}} \\ & + \lambda_{\text{decrease}} \mathcal{L}_{\text{decrease}} + \lambda_{\text{sparse}} \mathcal{L}_{\text{sparse}}. \end{aligned} \quad (9)$$

This yields a tokenizer that is content-adaptive, contrastively aligned with visual complexity, structurally monotonic for AR usage, and globally sparse under a controllable token budget. Further details on all loss terms and the corresponding weight settings are provided in the supplementary material.

3.3. Visual Generation with Adaptive Tokenizer

The primary purpose of visual tokenizers is to provide an effective representation space for generative models. To evaluate this capacity, we integrate STAT with a vanilla autoregressive (AR) model and train the AR model on the discrete latent tokens produced by STAT.

1-D autoregressive modeling. Given an image x , STAT produces a quantized latent sequence $q = (q_0, \dots, q_{L-1})$. The AR model is then trained to model the distribution over this sequence as:

$$p_\phi(z_q) = \prod_{t=0}^L p_\phi(z_t \mid z_{<t}), \quad (10)$$

where $p_\phi(\cdot)$ is the probability distribution parameterized by the AR model, and ϕ represents its learnable parameters.

EoS from keep probabilities. Different from traditional fixed-length tokenizers, STAT encodes each image together with a keep-probability profile $p = (p_0, \dots, p_{L-1})$, which is supposed to be nearly monotonic via $\mathcal{L}_{\text{decrease}}$ during the training of STAT (Sec. 3.2.2). This structure allows the AR model to operate in an adaptive manner using a special end-of-sequence (EoS) token. During training, we randomly sample a probability threshold τ and define the EoS position as:

$$k = \min\{i \mid p_i < \tau\}. \quad (11)$$

The AR model is then supervised on the prefix (z_0, \dots, z_{k-1}) followed by the EoS token. The monotonicity of p ensures that the thresholding is stable and naturally aligned with the soft tail-dropping behavior of STAT.

4. Experiments

In this section, we evaluate the reconstruction capacity of STAT, and explore its integration with an autoregressive (AR) generation model, assessing its effectiveness in both class-conditional and text-conditional image generation tasks. We show that STAT achieves higher reconstruction quality while using fewer tokens than existing visual tokenizers, demonstrating its ability to perform content-aware compression. For image generation, we demonstrate that a vanilla AR model combined with STAT attains competitive performance against both diffusion-based approaches and AR models that rely on complex training pipelines. Finally, we extend our study to the video domain and validate the effectiveness of the soft probabilistic tail-dropping mechanism for adaptive video tokenization.

Training setup. We train STAT on the ImageNet-1k [11] training set at a resolution of 256×256 using random-crop augmentation. The patch-embedding downsampling factor is set to $f = 16$, and the vector-quantizer uses a codebook of size 4096 with a code dimension of 12. The latent sequence length is set to 256. In the first stage, the keep length is sampled from a uniform distribution with bounds $L_{\min} = 160$ and $L_{\max} = 256$. At inference time, we use a default probability threshold of 0.5, retaining all tokens whose predicted keep probabilities exceed this threshold and dropping the rest. For additional hyperparameter settings and details of AR model training and inference, please refer to the supplementary material.

Metrics. We report reconstruction FID (rFID) [23] and PSNR for the image reconstruction task. For image generation, we evaluate generation FID (gFID) [23], Inception Score (IS) [50], and Precision/Recall [30]. For video reconstruction, we measure reconstruction FVD [59] (rFVD), PSNR, and LPIPS [70] to assess the quality.

4.1. Image Reconstruction

The evaluation for image reconstruction is conducted on the ImageNet-1K validation set at a resolution of 256×256 . We compare STAT with representative 2D and 1D tokenizers. As shown in Tab. 1, STAT achieves the best rFID among all tokenizers while using only 90% of the token count compared to other tokenizers. This highlights the benefits from the adaptive token allocation strategy learned by STAT, which maximizes the representational efficiency of the available tokens. Moreover, when allowing more token budgets for reconstruction by either adjusting the probability threshold in inference or manually adding the budgets, STAT shows further improvements in rFID, albeit with a marginal decrease in PSNR. We hypothesize that this trade-off emerges because more tokens encourage the model to prioritize perceptual realism over pixel-level fidelity.

In Fig. 4, we show the keep-probability profile for different images. We show that STAT successfully learns a



Figure 4. Keep-probability curves and corresponding reconstructions across samples of varying complexity. More complex images receive higher token counts, and the learned allocation correlates strongly with the JPEG file sizes of the inputs.

complexity-aware token allocation strategy, which is further validated by the high correlation between the allocated token counts and the JPEG sizes for storing the images.

Table 1. Comparison on ImageNet-1k image reconstruction. We compare with 2D image tokenizers including Taming VQ-GAN [16], MaskGIT VQ-GAN [5], Open MAGVIT-v2 [36], and the tokenizer in LlamaGen [56]; 1D image tokenizers including TiTok [68], FlexTok [2], and One-D-Piece [40]. All evaluations are performed on the ImageNet-1k validation set at a resolution of 256×256 . STAT achieves the best rFID while using 10% fewer tokens compared with other tokenizers. We additionally report results using a probability threshold of 0.01 at inference. “(+X Tokens)” denotes manually adding X extra tokens to all images at inference. These variants of STAT further improves to an rFID of 0.88 when using an average of 240 tokens.

Type	Tokenizer	#Tokens	Codebook Size	rFID ↓	PSNR ↑
2D Tokenizer	Taming VQ-GAN [16]	256	16384	4.98	19.40
	MaskGIT VQ-GAN [5]	256	1024	2.28	-
	Open MAGVIT-v2 [36]	256	262144	1.17	22.64
	LlamaGen [56]	256	4096	3.02	19.99
	LlamaGen [56]	256	16384	2.19	20.79
1D Tokenizer	TiTok-L [68]	32	4096	2.21	15.96
	TiTok-B [68]	64	4096	1.70	17.13
	TiTok-S [68]	128	4096	1.71	17.80
	FlexTok [2]	256	64000	1.08	17.70
	One-D-Piece-L [40]	256	4096	1.08	19.04
1D Tokenizer	STAT-Fixcount	220	4096	1.15	20.35
	STAT-Harddrop	222	4096	1.15	20.30
1D Tokenizer	STAT	220	4096	1.15	20.22
	STAT(Threshold 0.01)	230	4096	0.99	20.25
	STAT(Threshold 0.01; +10 Tokens)	240	4096	0.88	20.02

4.2. Image Generation

Given the strong reconstruction capability of STAT, we investigate whether this translates into improved generation performance. To this end, we integrate STAT into a vanilla autoregressive image generation framework, using the same backbone as LlamaGen [56]. An End-of-Sequence (EoS) token is used to allow the AR model to dynamically determine the effective token length during inference.

As summarized in Tab. 2, the vanilla AR model equipped with STAT achieves generation quality that is comparable to state-of-the-art AR and diffusion-based models, despite its minimalist design. This demonstrates that STAT is well suited for AR generative modeling, improving both efficiency and flexibility without requiring elaborate architectural heuristics. These results suggest that STAT not only

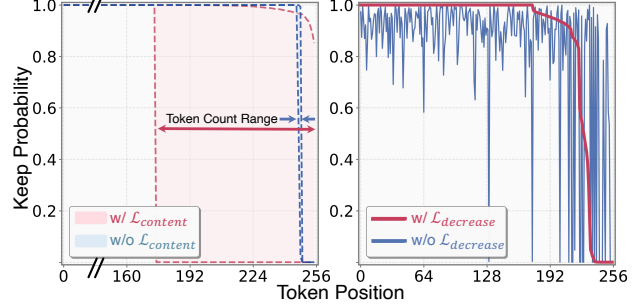


Figure 5. Ablation Study on the two loss terms for decreasing importance prior and the content-adaptive prior. The decreasing importance prior is necessary for learning the monotonic structure for AR generation, while the content-adaptive prior is crucial for successfully learning token allocation strategy.

excels at reconstruction, but also enhances generation in a simple AR setup, underscoring its potential as a strong tokenizer for generation and unified multimodal models.

In Tab. 3, we compare different visual tokenizers within the same AR generation framework, including the improved VQ tokenizer from LlamaGen, TiTok-S, and One-D-Piece-L. STAT delivers the best generation performance, surpassing all baseline tokenizers by a substantial margin. These results further confirm the effectiveness of STAT in enhancing autoregressive image generation.

4.3. Ablation Study

We investigate the effectiveness of different design components in the STAT pipeline, evaluating their impact on reconstruction and generation quality.

Adaptive Token Allocation. To assess whether the learned adaptivity contributes to performance gains, we include an ablation in which the tokenizer uses a fixed token count for all images. This count is set to the average number of tokens used by STAT in inference when the probability threshold is 0.5. We denote this variant as STAT-Fixcount.

The reconstruction comparison is shown in Tab. 1. While STAT-Fixcount achieves similar rFID and slightly higher PSNR, the adaptive version offers greater flexibility, enabling it to leverage additional token budgets to obtain im-

Table 2. **Comparison on ImageNet-1k class-conditional image generation.** We compare the AR generative model built on STAT with a broad range of generative models, including: GAN-based approaches such as BigGAN [3], GigaGAN [26], and StyleGAN [51]; diffusion-based models including ADM [12], LDM [49], DiT [42], and SiT [37]; autoregressive models with bi-directional attention including MaskGIT [5], MAGVIT-v2 [66], MAR [33], and TiTok [68]; autoregressive models with causal attention including VQGAN [16], RQTransformer [31], Open-MAGVIT-v2 [36], VAR [57], SAR [35], RAR [67], RandAR [41], and LlamaGen [56]. All evaluations are conducted on the ImageNet-1k validation set at a resolution of 256×256 . By simply replacing the original image tokenizer in LlamaGen with our proposed STAT, the 3B model achieves a gFID of 1.77, improving upon the LlamaGen baseline by 0.41 while using less than half the number of tokens. The performance of our AR model is also comparable to diffusion-based models and other AR models that rely on more advanced architectures and training strategies.

Type	Model	#Para.	gFID \downarrow	IS \uparrow	Precision \uparrow	Recall \uparrow	#Tokens
GAN	BigGAN [3]	112M	6.95	224.5	0.89	0.38	1
	GigaGAN [26]	569M	3.45	225.5	0.84	0.61	1
	StyleGAN-XL [51]	166M	2.30	265.1	0.78	0.53	1
Diffusion	ADM [12]	554M	4.59	186.7	0.82	0.53	250
	LDM-4 [49]	400M	3.60	247.7	—	—	250
	DiT-XL [42]	675M	2.27	278.2	0.83	0.57	250
	SiT-XL [37]	675M	2.06	270.3	0.82	0.59	250
Bi-directional AR	MaskGIT-re [5]	227M	4.02	355.6	—	—	256
	MAGVIT-v2 [66]	307M	1.78	319.4	—	—	256
	MAR-L [33]	479M	1.98	290.3	—	—	64
	MAR-H [33]	943M	1.55	303.7	0.81	0.62	256
	TiTok-S-128 [68]	287M	1.97	281.8	—	—	128
Advanced Causal AR	VAR [57]	600M	2.57	302.6	0.83	0.56	680
	VAR [57]	2.0B	1.92	350.2	0.82	0.59	680
	SAR-XL [35]	893M	2.76	273.8	0.84	0.55	256
	RAR-XXL [67]	955M	1.50	306.9	0.80	0.62	256
	RAR-XL [67]	1.5B	1.48	326.0	0.80	0.63	256
	RandAR-XL [41]	775M	2.25	317.8	0.80	0.60	256
	RandAR-XXL [41]	1.4B	2.15	322.0	0.79	0.62	256
Vanilla Causal AR	VQGAN [16]	1.4B	5.20	280.3	—	—	256
	RQTran.-re [31]	3.8B	3.80	323.7	—	—	256
	Open-MAGVIT-v2-XL [36]	1.5B	2.33	271.8	0.84	0.54	256
	LlamaGen-XL-256 [56]	775M	3.39	227.1	0.81	0.54	256
	LlamaGen-XXL-256 [56]	1.4B	3.09	253.6	0.82	0.53	576
	LlamaGen-3B-256 [56]	3.1B	3.06	279.7	0.84	0.54	576
	LlamaGen-XL-576 [56]	775M	2.62	244.1	0.80	0.57	576
	LlamaGen-XXL-576 [56]	1.4B	2.34	253.9	0.80	0.59	576
	LlamaGen-3B-576 [56]	3.1B	2.18	263.3	0.81	0.58	576
Vanilla Causal AR	LlamaGen-STAT-XL	775M	2.36	244.0	0.78	0.62	223
	LlamaGen-STAT-XXL	1.4B	1.91	290.2	0.79	0.63	227
	LlamaGen-STAT-3B	3.1B	1.75	300.6	0.80	0.64	229

proved rFID. For image generation results in Tab. 3), learning adaptivity leads to substantial performance gains. We attribute this improvement to that adaptive tokenization allows the AR model to jointly explore the latent code space and the token-count dimension, ultimately yielding higher-quality generations.

Per-Token v.s. Per-Sample Dropping. In STAT, token dropping is model as a per-token sampling process, and the proposed regularization terms shape the keep-probability profile into a soft tail-dropping pattern. To better under-

stand its effect, we implement a hard token dropping variant, dubbed STAT-Harddrop, in which tokens are always truncated from the tail, and the token count is determined by the sum of the predicted keep probabilities across all token positions.

As shown in Tab. 1, the two mechanisms show comparable performance, with STAT-Harddrop achieving slightly higher PSNR possibly due to the hard tail dropping pattern is easier for decoding. However, in image generation, STAT notably outperforms its harddrop counterpart. We at-

Table 3. **ImageNet-1k image class-conditional image generation performance on LlamaGen with different tokenizers.**

We train LlamaGen, a vanilla transformer-based autoregressive model, on different tokenizers including the VQ tokenizer in [56], TiTok [68], One-D-Piece [40], and STAT. All experiments are conducted on LlamaGen-XL (775M) with the same training settings. The model trained with STAT outperforms other tokenizers by a large margin. We further evaluate a variant that replaces the original soft probabilistic dropping strategy with a deterministic tail-drop, and the results demonstrate that the soft probabilistic dropping mechanism is essential for achieving high-quality generation.

Tokenizer	#Tokens	Codebook Size	gFID ↓	IS ↑	Pre. ↑	Rec. ↑
LlamaGen [56]	256	16384	3.39	227.1	0.81	0.54
LlamaGen [56]	576	16384	2.62	244.1	0.80	0.57
TiTok-S [68]	128	4096	4.90	191.7	0.77	0.56
One-D-Piece-L [40]	256	4096	2.99	235.1	0.81	0.59
STAT-FixCount	220	4096	2.73	234.2	0.77	0.62
STAT-Harddrop	223	4096	2.67	231.2	0.76	0.63
STAT-Fixthreshold	221	4096	2.49	240.7	0.79	0.61
STAT	223	4096	2.36	244.0	0.78	0.62

tribute this to the stochasticity introduced by per-token sampling where early tokens are also possibly dropped. This stochastic perturbation improves robustness to imperfect tokens and effectively mitigates the exposure bias commonly observed in autoregressive inference.

Position of the End-of-Sequence (EoS) Token. For the AR generation model, we examine whether sampling the EoS threshold and allowing its position to vary across different passes of the same images could lead to better performance than using a fixed threshold that enforces a static EoS position for each image. As in Tab. 3 between STAT and STAT-Fixthreshold, sampling the EoS threshold leads to a noticeable improvement in generation. The observation shows that the varying EoS positions could work as an augmentation for further improvement in generation.

Regularization Losses. We test the effectiveness of two loss terms: the decreasing loss and content-adaptive loss. As shown in Fig. 5, without the content-adaptive loss, the tokenizer is unable to learn effective token allocation strategies and learns only trivial solution where all images use almost the same token count. The decreasing loss is essential for the tokenizer to learn the soft tail dropping pattern and the structure prior of causality, which is necessary for AR generation training.

4.4. Text-conditional Image Generation

We evaluate STAT on text-conditional image generation by comparing it with the enhanced VQ tokenizer from LlamaGen [56]. Both tokenizers are trained on ImageNet, and we train separate vanilla autoregressive models with the two tokenizers on a subset of LAION-2B [52] for one epoch at the resolution 256×256. We measure the text-conditional generation quality on the GenEval [19] benchmark.

Table 4. **Comparison between STAT and VQGAN from LlamaGen on Text-conditional generation results on GenEval.**

Tokenizer	S. Obj.	T. Obj.	Count.	Colors	Position	C. Attri.	Overall
LlamaGen	0.91	0.18	0.19	0.57	0.04	0.01	0.32
STAT	0.99	0.36	0.40	0.81	0.10	0.06	0.45

Table 5. **Comparison on UCF-101 video reconstruction.** We compare STAT-Video with other video tokenizers including TATS [18], OmniTokenizer [63], ElasticTok [64], Cosmos-Tokenizer-DV [1], LARP [62], and AdapTok [34]. Following the evaluation protocol of AdapTok [34], all methods are evaluated on 16-frame video clips at a resolution of 128×128. Our approach achieves the best PSNR and LPIPS while delivering competitive FVD with other state-of-the-art video tokenizers. “(+ X Tokens)” denotes manually adding X extra tokens to all videos at inference. † indicates the baseline was trained for an additional 75 epochs.

Tokenizer	#Tokens	Codebook Size	rFVD ↓	PSNR ↑	LPIPS ↓
TATS [18]	1024	16384	157	24.22	0.206
OmniTokenizer [63]	1280	8192	62	27.76	0.112
ElasticTok [64]	1022	64000	230	-	-
Cosmos-Tokenizer-DV [1]	1280	64000	140	-	-
LARP [62]	1024	8192	24	-	-
LARP† [62]	1024	8192	20	28.71	0.075
AdapTok [34]	1024	8192	36	25.72	0.114
STAT-Video	997	8192	29	28.77	0.064
STAT-Video (+100 Tokens)	1097	8192	26	29.08	0.062
STAT-Video (+200 Tokens)	1197	8192	23	29.27	0.060
STAT-Video (+300 Tokens)	1297	8192	22	29.40	0.059

As shown in Tab. 4, STAT consistently outperforms the VQ model across all metrics, demonstrating stronger generalization for text-conditional generation.

4.5. Video Reconstruction

We extend our soft tail-dropping strategy to the video domain by applying STAT to 16-frame video clips. As shown in Tab. 5, STAT-Video achieves state-of-the-art reconstruction quality, obtaining the best PSNR and LPIPS among all compared video tokenizers, while also delivering competitive rFVD to prior state-of-the-art methods. Moreover, STAT-Video highlights the flexibility of adaptive tokenization: increasing the token budget consistently improves performance across all metrics, indicating that the proposed adaptive mechanism transfers effectively to the video domain and remains capable of learning content-dependent token allocation in spatiotemporal settings.

5. Conclusion

We present STAT, a content-adaptive 1D visual tokenizer with probabilistic tail dropping that aligns token length with content complexity via a contrastive objective. This design allows STAT to match or surpass state-of-the-art tokenizers in both reconstruction and generation while using fewer tokens. Our results show that adaptive, complexity-aware token cardinality serves as a strong inductive bias for high-dimensional generative modeling and could help enable unified multimodal autoregressive systems.

References

- [1] Niket Agarwal, Arslan Ali, Maciej Bala, Yogesh Balaji, Erik Barker, Tiffany Cai, Prithvijit Chattopadhyay, Yongxin Chen, Yin Cui, Yifan Ding, et al. Cosmos world foundation model platform for physical ai. *arXiv preprint arXiv:2501.03575*, 2025. 8
- [2] Roman Bachmann, Jesse Allardice, David Mizrahi, Enrico Fini, Oğuzhan Fatih Kar, Elmira Amirloo, Alaaeldin El-Nouby, Amir Zamir, and Afshin Dehghan. Flextok: Resampling images into 1d token sequences of flexible length. In *ICML*, 2025. 1, 2, 4, 6
- [3] Andrew Brock. Large scale gan training for high fidelity natural image synthesis. *arXiv preprint arXiv:1809.11096*, 2018. 2, 7
- [4] Di Chang, Hongyi Xu, You Xie, Yipeng Gao, Zhengfei Kuang, Shengqu Cai, Chenxu Zhang, Guoxian Song, Chao Wang, Yichun Shi, Zeyuan Chen, Shijie Zhou, Linjie Luo, Gordon Wetzstein, and Mohammad Soleymani. X-dyna: Expressive dynamic human image animation. In *CVPR*, 2025. 2
- [5] Huiwen Chang, Han Zhang, Lu Jiang, Ce Liu, and William T Freeman. Maskgit: Masked generative image transformer. In *CVPR*, 2022. 1, 2, 3, 6, 7
- [6] Mark Chen, Alec Radford, Rewon Child, Jeffrey Wu, Heewoo Jun, David Luan, and Ilya Sutskever. Generative pre-training from pixels. In *ICML*, 2020. 1, 2
- [7] Zeyuan Chen, Hongyi Xu, Guoxian Song, You Xie, Chenxu Zhang, Xin Chen, Chao Wang, Di Chang, and Linjie Luo. X-dancer: Expressive music to human dance video generation. In *ICCV*, 2025. 2
- [8] Zeyuan Chen, Xiang Zhang, Haiyang Xu, Jianwen Xie, and Zhuowen Tu. Cvp: Central-peripheral vision-inspired multi-modal model for spatial reasoning. In *WACV*, 2026. 1
- [9] Yufeng Cui, Honghao Chen, Haoge Deng, Xu Huang, Xinghang Li, Jirong Liu, Yang Liu, Zhuoyan Luo, Jinsheng Wang, Wenxuan Wang, Yueze Wang, Chengyuan Wang, Fan Zhang, Yingli Zhao, Ting Pan, Xianduo Li, Zecheng Hao, Wenxuan Ma, Zhuo Chen, Yulong Ao, Tiejun Huang, Zhongyuan Wang, and Xinlong Wang. Emu3.5: Native multimodal models are world learners, 2025.
- [10] Chaorui Deng, Deyao Zhu, Kunchang Li, Chenhui Gou, Feng Li, Zeyu Wang, Shu Zhong, Weihao Yu, Xiaonan Nie, Ziang Song, Guang Shi, and Haoqi Fan. Emerging properties in unified multimodal pretraining. *arXiv preprint arXiv:2505.14683*, 2025. 1, 3
- [11] Jia Deng, Wei Dong, Richard Socher, Li-Jia Li, Kai Li, and Li Fei-Fei. Imagenet: A large-scale hierarchical image database. In *CVPR*, 2009. 5, 3, 4
- [12] Prafulla Dhariwal and Alexander Nichol. Diffusion models beat gans on image synthesis. In *NeurIPS*, 2021. 7, 3
- [13] Shivam Duggal, Sanghyun Byun, William T Freeman, Antonio Torralba, and Phillip Isola. Single-pass adaptive image tokenization for minimum program search. In *NeurIPS*, 2025. 2
- [14] Shivam Duggal, Phillip Isola, Antonio Torralba, and William T Freeman. Adaptive length image tokenization via recurrent allocation. In *ICLR*, 2025. 2
- [15] Alaaeldin El-Nouby, Matthew J Muckley, Karen Ullrich, Ivan Laptev, Jakob Verbeek, and Hervé Jégou. Image compression with product quantized masked image modeling. *TMLR*, 2023. 2
- [16] Patrick Esser, Robin Rombach, and Bjorn Ommer. Taming transformers for high-resolution image synthesis. In *CVPR*, 2021. 2, 3, 6, 7
- [17] Shanghua Gao, Pan Zhou, Ming-Ming Cheng, and Shuicheng Yan. Masked diffusion transformer is a strong image synthesizer. In *ICCV*, 2023. 3, 4
- [18] Songwei Ge, Thomas Hayes, Harry Yang, Xi Yin, Guan Pang, David Jacobs, Jia-Bin Huang, and Devi Parikh. Long video generation with time-agnostic vqgan and time-sensitive transformer. In *ECCV*, 2022. 8
- [19] Dhruba Ghosh, Hannaneh Hajishirzi, and Ludwig Schmidt. Geneval: An object-focused framework for evaluating text-to-image alignment. *NeurIPS*, 2023. 8
- [20] Ian J Goodfellow, Jean Pouget-Abadie, Mehdi Mirza, Bing Xu, David Warde-Farley, Sherjil Ozair, Aaron Courville, and Yoshua Bengio. Generative adversarial nets. *NeurIPS*, 2014. 2
- [21] Jian Han, Jinlai Liu, Yi Jiang, Bin Yan, Yuqi Zhang, Zehuan Yuan, Bingyue Peng, and Xiaobing Liu. Infinity: Scaling bit-wise autoregressive modeling for high-resolution image synthesis, 2024. 3
- [22] D Hendrycks. Gaussian error linear units (gelus). *arXiv preprint arXiv:1606.08415*, 2016. 3
- [23] Martin Heusel, Hubert Ramsauer, Thomas Unterthiner, Bernhard Nessler, and Sepp Hochreiter. Gans trained by a two time-scale update rule converge to a local nash equilibrium. *NeurIPS*, 2017. 5
- [24] Jonathan Ho and Tim Salimans. Classifier-free diffusion guidance. *arXiv preprint arXiv:2207.12598*, 2022. 3
- [25] Jonathan Ho, Ajay Jain, and Pieter Abbeel. Denoising diffusion probabilistic models. *arXiv preprint arxiv:2006.11239*, 2020. 2
- [26] Minguk Kang, Jun-Yan Zhu, Richard Zhang, Jaesik Park, Eli Shechtman, Sylvain Paris, and Taesung Park. Scaling up gans for text-to-image synthesis. In *CVPR*, 2023. 2, 7
- [27] Dongwon Kim, Ju He, Qihang Yu, Chenglin Yang, Xiaohui Shen, Suha Kwak, and Liang-Chieh Chen. Democratizing text-to-image masked generative models with compact text-aware one-dimensional tokens. In *ICCV*, 2025. 1, 2, 3
- [28] Diederik P Kingma. Adam: A method for stochastic optimization. In *ICLR*, 2015. 3, 4
- [29] Diederik P Kingma and Max Welling. Auto-encoding variational bayes. *arXiv preprint arXiv:1312.6114*, 2013. 2
- [30] Tuomas Kynkänniemi, Tero Karras, Samuli Laine, Jaakko Lehtinen, and Timo Aila. Improved precision and recall metric for assessing generative models. *NeurIPS*, 2019. 5
- [31] Doyup Lee, Chiheon Kim, Saehoon Kim, Minsu Cho, and Wook-Shin Han. Autoregressive image generation using residual quantization. In *CVPR*, 2022. 2, 3, 7
- [32] José Lezama, Huiwen Chang, Lu Jiang, and Irfan Essa. Improved masked image generation with token-critic. In *ECCV*, 2022. 3

[33] Tianhong Li, Yonglong Tian, He Li, Mingyang Deng, and Kaiming He. Autoregressive image generation without vector quantization. In *NeurIPS*, 2024. 3, 7

[34] Yan Li, Changyao Tian, Renqiu Xia, Ning Liao, Weiwei Guo, Junchi Yan, Hongsheng Li, Jifeng Dai, Hao Li, and Xue Yang. Learning adaptive and temporally causal video tokenization in a 1d latent space. *arXiv preprint arXiv:2505.17011*, 2025. 8

[35] Wenze Liu, Le Zhuo, Yi Xin, Sheng Xia, Peng Gao, and Xiangyu Yue. Customize your visual autoregressive recipe with set autoregressive modeling. *arXiv preprint arXiv:2410.10511*, 2024. 7

[36] Zhuoyan Luo, Fengyuan Shi, Yixiao Ge, Yujiu Yang, Limin Wang, and Ying Shan. Open-magvit2: An open-source project toward democratizing auto-regressive visual generation. *arXiv preprint arXiv:2409.04410*, 2024. 6, 7

[37] Nanye Ma, Mark Goldstein, Michael S Albergo, Nicholas M Boffi, Eric Vanden-Eijnden, and Saining Xie. SIT: Exploring flow and diffusion-based generative models with scalable interpolant transformers. In *ECCV*, 2024. 7

[38] Yucheng Mao, Boyang Wang, Nilesh Kulkarni, and Jeong Joon Park. Sir-diff: Sparse image sets restoration with multi-view diffusion model. In *CVPR*, 2025. 2

[39] Fabian Mentzer, David Minnen, Eirikur Agustsson, and Michael Tschannen. Finite scalar quantization: Vq-vae made simple. In *ICLR*, 2024. 2

[40] Keita Miwa, Kento Sasaki, Hidehisa Arai, Tsubasa Takahashi, and Yu Yamaguchi. One-d-piece: Image tokenizer meets quality-controllable compression. *arXiv preprint arXiv:2501.10064*, 2025. 1, 2, 4, 6, 8

[41] Ziqi Pang, Tianyuan Zhang, Fujun Luan, Yunze Man, Hao Tan, Kai Zhang, William T Freeman, and Yu-Xiong Wang. Randar: Decoder-only autoregressive visual generation in random orders. In *CVPR*, 2025. 3, 7

[42] William Peebles and Saining Xie. Scalable diffusion models with transformers. In *ICCV*, 2023. 1, 2, 7

[43] Alec Radford, Karthik Narasimhan, Tim Salimans, Ilya Sutskever, et al. Improving language understanding by generative pre-training. 2018. 1, 2

[44] Alec Radford, Jeff Wu, Rewon Child, David Luan, Dario Amodei, and Ilya Sutskever. Language models are unsupervised multitask learners. 2019. 1

[45] Aditya Ramesh, Mikhail Pavlov, Gabriel Goh, Scott Gray, Chelsea Voss, Alec Radford, Mark Chen, and Ilya Sutskever. Zero-shot text-to-image generation. In *ICML*, 2021. 2

[46] Ali Razavi, Aaron Van den Oord, and Oriol Vinyals. Generating diverse high-fidelity images with vq-vae-2. *NeurIPS*, 2019. 2

[47] Sucheng Ren, Qihang Yu, Ju He, Xiaohui Shen, Alan Yuille, and Liang-Chieh Chen. Beyond next-token: Next-x prediction for autoregressive visual generation. In *ICCV*, 2025. 3

[48] Oren Rippel, Michael Gelbart, and Ryan Adams. Learning ordered representations with nested dropout. In *ICML*, 2014. 1, 2

[49] Robin Rombach, Andreas Blattmann, Dominik Lorenz, Patrick Esser, and Björn Ommer. High-resolution image synthesis with latent diffusion models. In *CVPR*, 2022. 2, 7

[50] Tim Salimans, Ian Goodfellow, Wojciech Zaremba, Vicki Cheung, Alec Radford, and Xi Chen. Improved techniques for training gans. *NeurIPS*, 2016. 5

[51] Axel Sauer, Katja Schwarz, and Andreas Geiger. Styleganxl: Scaling stylegan to large diverse datasets. In *SIGGRAPH*, 2022. 2, 7

[52] Christoph Schuhmann, Romain Beaumont, Richard Vencu, Cade Gordon, Ross Wightman, Mehdi Cherti, Theo Coombes, Aarush Katta, Clayton Mullis, Mitchell Wortsman, et al. Laion-5b: An open large-scale dataset for training next generation image-text models. *NeurIPS*, 2022. 8

[53] Rico Sennrich, Barry Haddow, and Alexandra Birch. Neural machine translation of rare words with subword units. In *ACL*, 2016. 1

[54] Jiaming Song, Chenlin Meng, and Stefano Ermon. Denoising diffusion implicit models. In *ICLR*, 2021. 2

[55] Jianlin Su, Murtadha Ahmed, Yu Lu, Shengfeng Pan, Wen Bo, and Yunfeng Liu. Roformer: Enhanced transformer with rotary position embedding. *Neurocomputing*, 2024. 3

[56] Peize Sun, Yi Jiang, Shoufa Chen, Shilong Zhang, Bingyue Peng, Ping Luo, and Zehuan Yuan. Autoregressive model beats diffusion: Llama for scalable image generation. *arXiv preprint arXiv:2406.06525*, 2024. 1, 3, 6, 7, 8

[57] Keyu Tian, Yi Jiang, Zehuan Yuan, Bingyue Peng, and Liwei Wang. Visual autoregressive modeling: Scalable image generation via next-scale prediction. In *NeurIPS*, 2024. 3, 7

[58] Hugo Touvron, Thibaut Lavril, Gautier Izacard, Xavier Martinet, Marie-Anne Lachaux, Timothée Lacroix, Baptiste Rozière, Naman Goyal, Eric Hambro, Faisal Azhar, et al. Llama: Open and efficient foundation language models. *arXiv preprint arXiv:2302.13971*, 2023. 1

[59] Thomas Unterthiner, Sjoerd Van Steenkiste, Karol Kurach, Raphael Marinier, Marcin Michalski, and Sylvain Gelly. Towards accurate generative models of video: A new metric & challenges. *arXiv preprint arXiv:1812.01717*, 2018. 5

[60] Aaron Van Den Oord, Oriol Vinyals, et al. Neural discrete representation learning. *NeurIPS*, 2017. 2

[61] Ashish Vaswani, Noam Shazeer, Niki Parmar, Jakob Uszkoreit, Llion Jones, Aidan N Gomez, Łukasz Kaiser, and Illia Polosukhin. Attention is all you need. *NeurIPS*, 2017. 3

[62] Hanyu Wang, Saksham Suri, Yixuan Ren, Hao Chen, and Abhinav Shrivastava. Larp: Tokenizing videos with a learned autoregressive generative prior. *arXiv preprint arXiv:2410.21264*, 2024. 8

[63] Junke Wang, Yi Jiang, Zehuan Yuan, Bingyue Peng, Zuxuan Wu, and Yu-Gang Jiang. Omnitokenizer: A joint image-video tokenizer for visual generation. *NeurIPS*, 2024. 8

[64] Wilson Yan, Volodymyr Mnih, Aleksandra Faust, Matei Zaharia, Pieter Abbeel, and Hao Liu. Elastictok: Adaptive tokenization for image and video. *ICLR*, 2025. 2, 8

[65] Jiahui Yu, Xin Li, Jing Yu Koh, Han Zhang, Ruoming Pang, James Qin, Alexander Ku, Yuanzhong Xu, Jason Baldridge, and Yonghui Wu. Vector-quantized image modeling with improved vqgan. *arXiv preprint arXiv:2110.04627*, 2021. 2, 3

[66] Lijun Yu, José Lezama, Nitesh B. Gundavarapu, Luca Verzani, Kihyuk Sohn, David Minnen, Yong Cheng, Vignesh Birodkar, Agrim Gupta, Xiuye Gu, Alexander G.

Hauptmann, Boqing Gong, Ming-Hsuan Yang, Irfan Essa, David A. Ross, and Lu Jiang. Language model beats diffusion–tokenizer is key to visual generation. In *ICLR*, 2024. 2, 3, 7

[67] Qihang Yu, Ju He, Xueqing Deng, Xiaohui Shen, and Liang-Chieh Chen. Randomized autoregressive visual generation. *arXiv preprint arXiv:2411.00776*, 2024. 7, 3

[68] Qihang Yu, Mark Weber, Xueqing Deng, Xiaohui Shen, Daniel Cremers, and Liang-Chieh Chen. An image is worth 32 tokens for reconstruction and generation. *NeurIPS*, 2024. 1, 2, 6, 7, 8, 3

[69] Guanning Zeng, Xiang Zhang, Zirui Wang, Haiyang Xu, Zeyuan Chen, Bingnan Li, and Zhuowen Tu. Yolo-count: Differentiable object counting for text-to-image generation. In *ICCV*, 2025. 2

[70] Richard Zhang, Phillip Isola, Alexei A Efros, Eli Shechtman, and Oliver Wang. The unreasonable effectiveness of deep features as a perceptual metric. In *CVPR*, 2018. 5

[71] Yue Zhao, Yuanjun Xiong, and Philipp Krahenbuhl. Image and video tokenization with binary spherical quantization. In *ICLR*, 2025. 2

[72] Chunting Zhou, Lili Yu, Arun Babu, Kushal Tirumala, Michihiro Yasunaga, Leonid Shamis, Jacob Kahn, Xuezhe Ma, Luke Zettlemoyer, and Omer Levy. Transfusion: Predict the next token and diffuse images with one multi-modal model. *arXiv preprint arXiv:2408.11039*, 2024. 3

Soft Tail-dropping for Adaptive Visual Tokenization

Supplementary Material

In the supplementary material, we begin with analyzing the token count distribution and its relationship to JPEG file size in Sec. 6. Next, we provide additional quantitative and qualitative results in Secs. 7, 8, and 9. Finally, we discuss the limitations of STAT in Sec. 10 and present full implementation details in Sec. 11.

6. Token Count and JPEG Size

We conduct inference on the ImageNet-1k validation set, which contains 50,000 images. For each image, we record its JPEG file size and use STAT to compute the expected token count for decoding by summing the per-position keep probabilities. The visualization in Fig. 6 shows a clear and strong correlation between JPEG size and the predicted token count. This implies that STAT implicitly models frequency-domain complexity—assigning more tokens to images with rich high-frequency content (e.g., textures, edges) and fewer tokens to smoother regions, despite not being trained with any explicit frequency supervision.

We further fit a linear regression to quantify this relationship and obtain the following equation between the expected token count and the JPEG file size:

$$\text{Token-Count} = 0.44 \times \text{JPEG-Size (KB)} + 167.6. \quad (12)$$

This suggests that increasing the token budget by one token corresponds to encoding roughly an additional 2 KB of information measured under the JPEG compression scheme.

7. Ablation Study on STAT Inference

We ablate how STAT determines the token count *in inference* using the predicted per-token keep probabilities. By default, we apply a threshold of 0.5 and discard all tokens whose keep probabilities fall below this value. As an alternative, we compute the expected number of retained tokens by summing all keep probabilities for an image, and then keep only the first tokens up to this expected count, truncating the remaining tail tokens. Since STAT imposes a decreasing importance prior that enforces a monotonic decay in keep probabilities, the behaviors of the thresholding and expectation-based strategies are similar. The results are reported in Tab. 6, which show that once the average token counts are matched across the two inference strategies, their reconstruction performance is very close.

8. Image Reconstruction at 512×512

We further evaluate the feasibility of STAT at a resolution of 512×512 on ImageNet. All settings remain unchanged

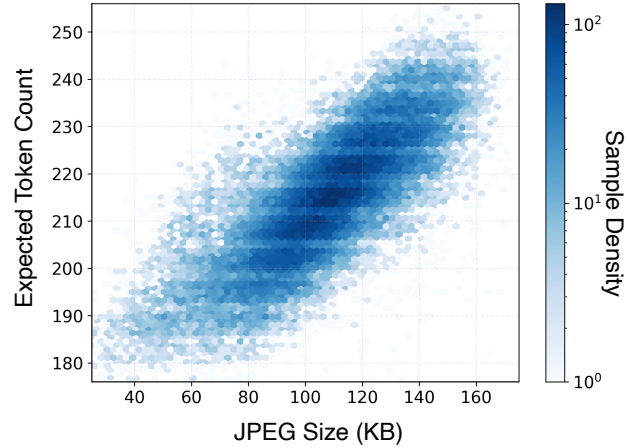


Figure 6. Visualization of JPEG file size versus the expected token count predicted by our adaptive tokenizer. We evaluate 50,000 ImageNet-1k validation images, with each hexagonal bin showing the log-density of samples. The strong correlation indicates that STAT effectively aligns token allocation with the underlying image complexity reflected by JPEG size.

Table 6. **Comparison on ImageNet-1k image reconstruction.** Ablation of inference-time settings in STAT.

Tokenizer	#Tokens	rFID \downarrow	PSNR \uparrow
STAT(threshold 0.5)	220	1.15	20.22
STAT(expected token count)	216	1.20	20.21
STAT(expected token count; +4 tokens)	220	1.14	20.24

Table 7. **Comparison on ImageNet-1k image reconstruction at the resolution of 512×512 .**

Tokenizer	#Tokens	Codebook Size	rFID \downarrow	PSNR \uparrow
MaskGIT VQ-GAN [5]	1024	1024	1.97	-
TiTok-L-64 [68]	64	4096	1.77	-
TiTok-B-128 [68]	128	4096	1.52	-
LlamaGen [56]	1024	16384	0.70	23.03
STAT(threshold 0.5)	471	4096	0.87	20.98
STAT(threshold 0.01)	482	4096	0.82	20.98
STAT(threshold 0.01; +20 tokens)	501	4096	0.75	20.88

except that we double the latent sequence length to accommodate higher-resolution reconstructions. The results are reported in Tab. 7. STAT achieves an rFID competitive with the tokenizer used in LlamaGen [56], while using a smaller codebook and less than half the average number of tokens. We note that the PSNR of STAT is lower than that of LlamaGen, likely because the model is bottlenecked by both the codebook size and the number of tokens, which limits its ability to recover all fine-grained details. Nevertheless, the



Figure 7. **Limitation of STAT.** Increasing the token count beyond the amount allocated by STAT does not always improve reconstruction faithfulness, as seen in the artifacts in the pumpkin’s eye and the color distortions in the heron sample when reconstructed with 256 tokens.

low rFID indicates that STAT is still capable of producing high-quality reconstructions at a higher resolution.

9. Qualitative Results

We present qualitative results on image reconstruction, class-conditional image generation, and text-conditional image generation from page 5 to page 8.

9.1. Image Reconstruction

The reconstruction results of STAT with varying token counts are shown in Fig. 8. As illustrated, STAT naturally assigns larger token counts to visually complex images. From top to bottom, reconstructions with fewer tokens exhibit blurry regions or missing fine details (e.g., the rightmost two samples), while increasing the token counts progressively restores clear structures and sharp textures.

9.2. Text-conditional Image Generation

We show text-conditional image generation results in Fig. 9. All generations are at a resolution of 256×256 . The results demonstrate that a vanilla autoregressive model paired with STAT achieves strong text-conditional generation quality.

9.3. Class-conditional Image Generation

The class-conditional image generation results are shown in Fig. 10. Our autoregressive model achieves a FID of 1.74 on ImageNet, and the qualitative results illustrate its capability to generate visually compelling and diverse images.

9.4. Adaptive Image Generation

Fig. 11 shows that the adaptivity of STAT enables the autoregressive model to perform adaptive image generation as well: the model can generate plausible images with as few as 160 tokens, while allocating more tokens progressively enhances realism and detail. This mirrors the adaptive behavior of STAT in image reconstruction.

10. Limitations

We observe that when the token count used for reconstructing an image deviates significantly from the token count allocated by STAT, quality degrades. Using too few tokens naturally leads to poor reconstructions, but using too many tokens can also introduce artifacts and color distortions. Representative examples are provided in Fig. 7.

In text-conditional generation, our model still faces challenges such as imperfect text rendering, structural inconsistencies, and mismatches between the generated content and the input prompts. These issues primarily stem from limitations in the scale and quality of available training data, as well as our computational budget. We expect that larger, higher-quality datasets and increased compute will help alleviate these shortcomings.

Finally, in this work we evaluate only the reconstruction capabilities of STAT on videos and on images at 512×512 resolution. Exploring the generation performance of STAT with autoregressive models on videos and at even higher image resolutions would be a direction for future work.

11. Implementation Details

We provide implementation and training details for STAT in Sec. 11.1 and for autoregressive generative models in Sec. 11.2. All training and inference code, along with model checkpoints, will be released for research purposes.

11.1. STAT Details

As described in the main paper, STAT is trained in two stages. Tab. 8 and Tab. 9 summarize the full model configurations and training hyperparameters for each stage.

Loss Functions. We use a reconstruction loss $\mathcal{L}_{\text{recon}} = \mathcal{L}_{\text{L2}} + \mathcal{L}_{\text{perceptual}}$, which combines an L2 loss with a perceptual loss to improve visual fidelity. A GAN loss \mathcal{L}_{GAN} is included to further enhance reconstruction quality, and a VQ loss \mathcal{L}_{VQ} is applied to optimize the codebook. The total

loss for the first stage is defined as

$$\mathcal{L}_{\text{stage1}} = \mathcal{L}_{\text{recon}} + \mathcal{L}_{\text{GAN}} + \mathcal{L}_{\text{VQ}}, \quad (13)$$

where loss weights are omitted for simplicity.

In the second stage, we additionally introduce three regularization losses to learn adaptive token allocation, yielding

$$\begin{aligned} \mathcal{L}_{\text{stage1}} = & \mathcal{L}_{\text{recon}} + \mathcal{L}_{\text{GAN}} + \mathcal{L}_{\text{VQ}} \\ & + \mathcal{L}_{\text{content}} + \mathcal{L}_{\text{decrease}} + \mathcal{L}_{\text{sparse}}, \end{aligned} \quad (14)$$

again omitting the weighting parameters. Please refer to Tab. 8 and Tab. 9 for the exact weighting values used in both stages. The loss weights are chosen such that the maximum token count allocated by STAT approximately matches the full sequence length (256). For the KL sparsity prior loss $\mathcal{L}_{\text{sparse}}$, we set the target sparsity to $p^* = 0.5$.

Architecture of the Probability Head. In the second stage, STAT employs a probability head to predict per-token keep probabilities. This head is implemented as a position-aware multi-layer perceptron (MLP) with a final sigmoid activation. The MLP consists of a linear layer, a GELU [22] activation, and another linear layer. To incorporate positional information, sinusoidal positional embeddings [61] are added to the input before it is fed into the MLP.

11.2. Autoregressive Model Details

We train three variants of autoregressive models with sizes XL (775M), XXL (1.4B), and 3B (3.1B). Their architectural configurations follow LlamaGen [56], except that we replace the 2D RoPE [55] with a 1D version to match the 1D token sequence produced by STAT.

Position of the End-of-Sequence (EoS) Token. During training, we dynamically sample a threshold in each forward pass to determine the EoS position. We maintain a set of fixed thresholds $[0.99, 0.5, 0.25, 0.1, 0.01, 0.001]$. With 75% probability, we randomly draw a threshold from this set, and the first token position whose predicted keep probability falls below this threshold is marked as the EoS. For the remaining 25% of iterations, we instead sample a threshold uniformly from $(0, 1)$ and determine the EoS position in the same way. Note that this threshold-based EoS sampling is valid only because the keep probability profile is enforced to be non-increasing by the importance decreasing prior used when training STAT.

Loss Computation. The autoregressive model is trained using cross-entropy loss. Once the EoS position is identified, all tokens beyond the EoS are padded and excluded in the computation of the loss, as they provide no meaningful supervision under the chosen decoding length.

Sampling Protocols. For FID evaluation, we generate 50,000 images and compute the metric with the code from [12]. Classifier-free guidance [24] is applied during sampling. Following RAR [67], we adopt the power-cosine

Table 8. **Hyperparameters for the first-stage training of STAT.** Most settings follow TiTok [68] and TA-TiTok [27], except that our transformer decoder is trained to directly predict pixels rather than discrete codes of MaskGIT VQ-GAN in TiTok.

Item	Value
Model	
Codebook Size	4,096
Token Size	12
Model Size	ViT Large
Patch Size	16
Latent Sequence Length	256
Training	
Epochs	100
Batch Size	1024
Dataset	ImageNet-1k [11]
Augmentation	Random Crop / Flip
Losses	
L2 Reconstruction Weight	1.0
Quantizer Weight	1.0
Perceptual Loss Model	ConvNeXT-Small [Link]
Perceptual Loss Weight	1.1
Codebook Loss Weight	1.0
Commitment Loss Weight	0.25
Discriminator Loss Start	Epoch 80
Discriminator Weight	0.1
Lecam Regularization Weight	0.001
Optimizer	
Optimizer	AdamW [28]
Learning Rate (LR)	1e-4
Discriminator LR	1e-4
Beta1	0.9
Beta2	0.999
Weight Decay	1e-4
Epsilon	1e-8
Scheduler	
Scheduler Type	Cosine
Warmup Steps	10,000
End Learning Rate	1e-5

guidance schedule [17]. We do not apply any top- k or top- p filtering techniques.

Please find all figures on the following pages.

Table 9. **Hyperparameters for the second stage training of STAT.** We use a lower learning rate for the probability head to ensure a more stable training process.

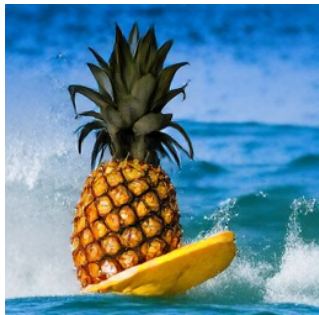
Item	Value
Model	
Codebook Size	4,096
Token Size	12
Model Size	ViT Large
Patch Size	16
Latent Sequence Length	256
Training	
Epochs	160
Batch Size	1024
Dataset	ImageNet-1k [11]
Augmentation	Random Crop / Flip
Losses	
L2 Reconstruction Weight	1.0
Quantizer Weight	1.0
Perceptual Loss Model	ConvNeXT-Small [Link]
Perceptual Loss Weight	1.1
Codebook Loss Weight	1.0
Commitment Loss Weight	0.25
Discriminator Loss Start	Epoch 20
Discriminator Weight	0.1
Lecam Regularization Weight	0.001
Rank Weight	1.0
Decreasing Loss Weight	50.0
Sparse Loss Weight	0.005
Optimizer	
Optimizer	AdamW [28]
Learning Rate (LR)	5e-5
Probability Head LR	1e-5
Discriminator LR	5e-5
Beta1	0.9
Beta2	0.999
Weight Decay	1e-4
Epsilon	1e-8
Scheduler	
Scheduler Type	Cosine
Warmup Steps	10,000
End Learning Rate	1e-5

Table 10. **Hyperparameters for the autoregressive models.**

Item	Value
Model	
Layers	36 (XL) / 48 (XXL) / 24 (3B)
Hidden Size	1280 (XL) / 1536 (XXL) / 3200 (3B)
Heads	20 (XL) / 24 (XXL) / 32 (3B)
Training	
Epochs	400 (XL) / 640 (XXL) / 800 (3B)
Batch Size	512 (XL) / 1024 (XXL) / 1024 (3B)
Dataset	ImageNet-1k [11]
Optimizer	AdamW [28]
Learning Rate	1e-4
Sampling	
Guidance Schedule	pow-cosine [17]
Temperature	1.0
Scale Power	2.5 (XL) / 1.2 (XXL) / 1.15 (3B)
Guidance Scale	18.0 (XL) / 7.0 (XXL) / 12.0 (3B)



Figure 8. **Adaptive image reconstruction with STAT.** Bottom labels indicate the allocated tokens. Each row shows reconstructions using a fixed token count (left), while the last two rows depict results using the token counts predicted by STAT and the original input images.



A pineapple surfing on a wave



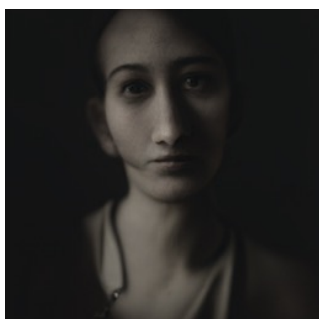
A colorful coral reef bustling with marine life



A painting of a fox in the style of starry night



A snowy mountain peak with blue sky



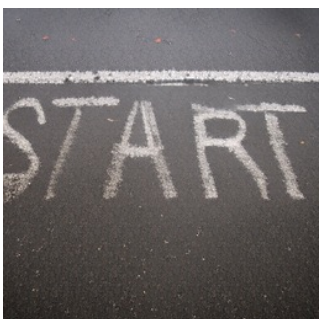
A woman in a minimalistic studio portrait



A steampunk airship floating above a Victorian-era city



A painting of a sport car in the style of Monet



The word "START" written on a street surface



A cozy cabin interior with a fireplace during a snowstorm



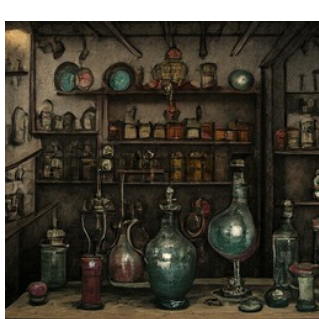
Yin-yang



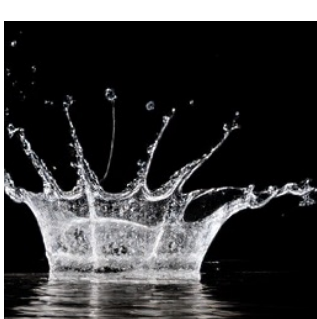
An illustration of a teapot



A wolf standing on a snowy ridge during golden hour



A medieval alchemist's laboratory filled with mysterious potions



A high-speed photograph of a splash forming a crown shape



A watercolor painting of a small European village by a river



A vintage red sports car parked on a coastal highway at sunset

Figure 9. Text-conditional 256×256 Image Generation. The input text prompts are shown below the images.



Class id 207: Golden retriever



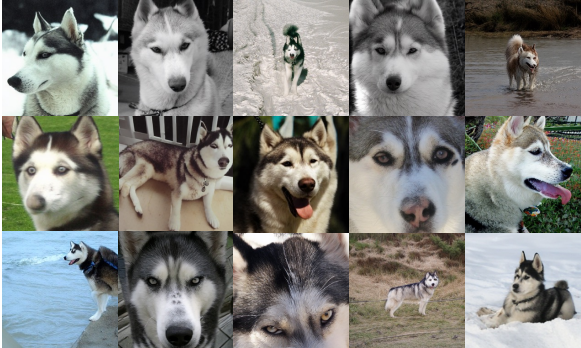
Class id 973: Coral reef



Class id 562: Fountain



Class id 417: Balloon



Class id 250, Siberian husky



Class id 975: Lakeside



Class id 928: Ice cream



Class id 980: Volcano

Figure 10. **Class-conditional 256×256 Image Generation.** Each block shows samples generated for a specific ImageNet class, labeled with its class id and name. Combined with STAT, a vanilla autoregressive generative model achieves strong diversity and fidelity.

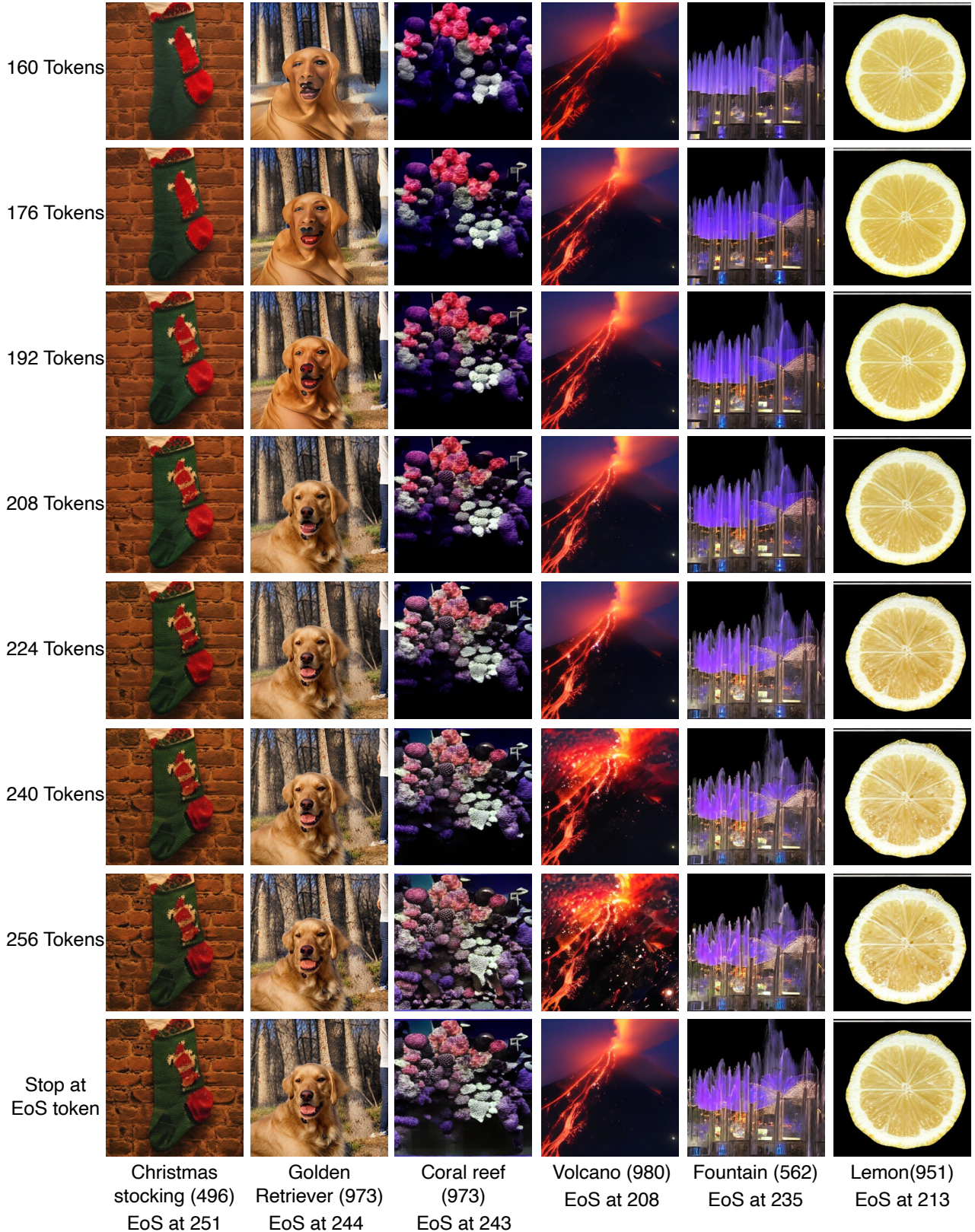


Figure 11. **Adaptive Image Generation with STAT.** Bottom labels show the class name and the predicted End-of-Sequence (EoS) position for each sample. Rows show images generated with fixed token budgets or the token counts determined by the EoS position.